

High-gradient performance of a prototype accelerator cavity for a 3 GeV proton radiography booster

Muhammed Zuboraj^{✉,*}, Yuri K. Batygin[✉], Sergey S. Kurennoy[✉], Eric R. Olivas, Evgenya I. Simakov[✉], and Haoran Xu

Los Alamos National Laboratory, P.O. Box 1663, Los Alamos, New Mexico 87545, USA



(Received 7 September 2023; accepted 8 January 2024; published 5 February 2024)

This paper reports the design, fabrication, and results of the high-gradient conditioning and testing for a two-cell, π -mode, standing wave normal-conducting prototype booster cavity for the proposed 3 GeV proton linac upgrade at Los Alamos Neutron Science Center. Increasing the energy of proton beam from the existing 800 MeV to 3 GeV will improve resolution of the proton radiography by up to 10 times. The proposed energy boost can be achieved with a compact normal-conducting high-gradient radio-frequency (rf) linac section. The C-band section of the booster linac was designed with optimized-shaped copper accelerator cavities with distributed rf coupling. A short two-cell test prototype structure was designed for the frequency of 5.712 GHz, fabricated, and tested at the C-band Engineering Research Test Facility in New Mexico (CERF-NM) at Los Alamos National Laboratory. The maximum klystron power coupled into the test structure was 8.3 MW with 1 μ s pulse length and 100 Hz repetition rate. The breakdown probabilities were recorded as functions of the accelerating gradient and peak surface fields. Operation of the test cavity at accelerating gradients of up to 100 MV/m was demonstrated.

DOI: [10.1103/PhysRevAccelBeams.27.021001](https://doi.org/10.1103/PhysRevAccelBeams.27.021001)

I. INTRODUCTION

Proton radiography (pRad) has been an integral program at Los Alamos Neutron Science Center (LANSCE) for the last 30 years [1]. It aims to probe materials under extreme conditions through static and dynamic experiments. The current LANSCE pRad operates with an 800 MeV proton beam provided by the LANSCE linac. It produces single images and short movies with several tens of frames. Each short pRad beam pulse consists of several successive bunches from the linac, coming at the drift tube linac (DTL) repetition frequency of 201.25 MHz. Using multiple bunches to produce the image increases the total intensity of the pulse that is limited by the bunch current (10 mA) at 800 MeV, constrained by the capabilities of the ion source at the front end and losses along the linac. To prevent image blur, the total length of the pRad macropulse is restricted to 80 ns or the total of 16 linac bunches.

Currently, Los Alamos National Laboratory (LANL) recognized the critical need to improve the capabilities of proton radiography, particularly image resolution [2]. The most effective pathway to improving the image resolution

is through increasing the incident proton energy [3,4]. There are several reasons for that. The radiography resolution of a pRad system is limited by two factors: the second-order chromatic aberration terms in the magnetic lens which is the primary source of image blur and the energy and angle spread of the protons due to the energy loss and multiple Coulomb scattering within the object. Increasing the proton beam energy from 800 MeV to 3 GeV increases the beam momentum p by a factor of 2.6. The chromatic blur scales with the beam momentum as $1/p^2$ [5], while the in-object scattering blur scales as $1/p$ [3]. Therefore, increasing the energy of the proton beam at LANSCE from 800 MeV to 3 GeV will improve radiography resolution by tenfold for imaging thinner objects while also allowing to image thicker objects.

Several pathways toward increasing the energy of LANSCE proton beam from 800 MeV to 3 GeV were considered. The needed energy boost can be achieved either with a proton synchrotron or with a proton linac. The synchrotron option for the pRad upgrade at LANSCE could be analogous to the Schwerionensynchrotron (SIS) heavy ion synchrotron at Gesellschaft für Schwerionenforschung (GSI) Helmholtz Center for Heavy Ion Research [6–8]. The synchrotron option allows more protons per bunch and comes with possibilities to extract proton bunches at an arbitrary, intermediate energy level. However, for the proton synchrotron solution, the time interval between two proton pulses is constrained to discretized values which does not provide enough flexibility as desired for

*zuboraj@lanl.gov

Published by the American Physical Society under the terms of the [Creative Commons Attribution 4.0 International license](https://creativecommons.org/licenses/by/4.0/). Further distribution of this work must maintain attribution to the author(s) and the published article's title, journal citation, and DOI.

the pRad upgrade [2]. An additional significant challenge is posed by the requirement to have a reliable fast kicker [9] with a rise time of less than 50 ns to produce the bunch train relevant to pRad. In comparison, for the linac option, the number of bunches (including single-bunch operation), bunch length, and intervals between the bunches are directly controlled by the fast chopper with a typical rise time of less than 10 ns [10,11] at the lower-energy end of the LANSCE linac.

We considered both the superconducting radiofrequency (SRF) and the normal conducting radiofrequency (NCRF) proton linacs as possible linac upgrade options. However, it was realized early on that employing an SRF linac with typical operational accelerating gradients of 15 MV/m or lower would lead to a 150-m-long accelerating structure length needed to achieve the desired energy boost, which would require significant expensive modifications of the existing beam tunnel [3]. Moreover, pRad at LANSCE works at a very low duty factor [12] with typically less than ten proton bunch trains required in a day of operations, making the SRF option not cost-efficient.

All above said, it was proposed to employ a normal conducting radiofrequency booster linac [12]. The proposed booster linac architecture described in detail in [13,14] includes a C- (or X-) band main linac section that provides the main acceleration from 1.6 GeV to the final energy of 3 GeV. The 5635 MHz, C-band section of the pRad booster linac must meet two requirements: a beam aperture large enough to provide sufficient acceptance of the proton beam coming from the existing LANSCE linac [14] and a shunt impedance of the accelerating structure that is sufficiently high to deliver the required acceleration over the length shorter than 50 m and stay within reasonable power requirements. The acceptance requirement follows from beam dynamics considerations described in [14]. For the C-band booster section, the minimum value of the aperture radius a_{\min} depends on the beam velocity and energy as

$$a_{\min} \approx \frac{10}{\sqrt{\beta\gamma}} \text{ [mm]}. \quad (1)$$

For the 1.6 GeV proton kinetic energy, meaning velocity $\beta = 0.93$ and the Lorentz factor $\gamma = 2.72$, Eq. (1) leads to $a_{\min} \approx 6.3$ mm. Therefore, in the finalized test cavity design, the beam aperture radius $a = 6.5$ mm was selected [15]. Next, based on the final energy and the rf power considerations, it was decided that the 50-m-long C-band linac should operate at a gradient of 40 MV/m.

In recent years, several C-band accelerating structures have been designed, tested, and employed to accelerate electron beams at other institutions. The structures had comparable apertures and were designed to operate in the traveling-wave (TW) mode. Istituto Nazionale di Fisica Nucleare (INFN) developed the traveling-wave $2\pi/3$ accelerating structure for the SPARC-LAB linac energy

upgrade [16–18]. The structure reported in [16] had a very high-shunt impedance of 82.8 M Ω /m. The structure reported in [17,18] had silicon carbide absorbers for the higher-order-mode damping which resulted in a slightly lower shunt impedance of 70 M Ω /m. RIKEN SPring-8 developed the traveling-wave $2\pi/3$ accelerating structure with an even larger beam aperture but a lower shunt impedance of 66 M Ω /m for the angstrom compact free-electron laser [19]. Shanghai Institute of Applied Physics (SINAP) demonstrated the TW $4\pi/5$ accelerating structure with the same larger aperture for the free-electron laser facility at the Shanghai Institute of Applied Physics (SINAP) with the shunt impedance of 62 M Ω /m [20].

High-gradient C-band hadron linac structures have been researched, developed, and tested previously for hadron therapy purposes [21–23]. A typical accelerating structure for hadron therapy represents a side-coupled linac working in a $\pi/2$ mode, the side coupling allows for reducing the diameter of the beam hole to a few millimeters and maximizes the shunt impedance. The structures reported in [21–23] have shunt impedances of 100 M Ω /m or even higher that are achieved by employing very small beam holes together with the nose-cone geometry that comes at the expense of very high-peak surface electric fields in the structure. Compared to those structures, the unique C-band booster linac cavity design described in this paper utilizes a distinctly larger beam aperture, with a high-shunt impedance retained.

To satisfy the large aperture and high-shunt impedance requirements, we employed a distributed coupling scheme [24] for the C-band booster linac cavities [15]. The distributed coupling topology allowed us to optimize cavity shapes for power consumption and efficiency and for reduction of the surface peak fields. For example, as reported in [25], the traveling-wave $2\pi/3$ C-band accelerating structure designed to operate in-resonance with slower than the speed-of-light, $\beta = 0.93$, beam would have the shunt impedance that is 2 times smaller than the proposed distributed-coupling structure and notably higher peak surface electric fields.

To confirm that the new design of the C-band booster linac cavity will meet the operational requirements for pRad upgrade, e.g., will attain the desired accelerating gradient with acceptable breakdown probability, we proceeded to conduct high-gradient tests of the proposed structure. For the simple high-gradient test, we designed a two-cell test structure [15] with a distributed coupling scheme. The test structure was scaled to a slightly higher frequency of 5712 MHz for compatibility with LANL's C-band Engineering Research Facility in New Mexico (CERF-NM) high gradient rf structure test stand [26,27].

In this paper, we report the electromagnetic and mechanical designs of the two-cell C-band test structure, the results of the low power rf tests and tuning, and the high-gradient test results. The measured breakdown probabilities of the test cavity are reported, as a function of the

accelerating gradient and of the peak fields. The organization of the paper is as follows. Section II presents the design of the two-cell cavity and describes its fabrication. Section III describes the cold test and tuning of the cavity. Section IV covers the high-gradient conditioning setup and the process of the high-gradient conditioning of the two-cell structure. Section V presents and discusses the breakdown statistics collected at the end of the high-gradient conditioning. Section VI is the conclusion.

II. DESIGN OF THE C-BAND TEST CAVITY FOR PRAD PROTON BOOSTER

A two-cell, π -mode, standing wave test cavity for the pRad booster linac study was designed at the frequency of $f = 5.712$ GHz, with distributed rf coupling. The CST Microwave Studio (MWS) model of the test cavity is shown in Fig. 1(a). The distribution of the longitudinal component of the electric field (E_z) in the π mode of the cavity is illustrated in Fig. 1(b). The input rf power enters the cavity through the WR187 waveguide. A taper section matches the WR187 port to the main waveguide. The width of the main waveguide is designated as w and is calculated from geometrical considerations of achieving coupling into the π mode as described below. The length of each cavity, L_c , is determined by the requirement to be in resonance

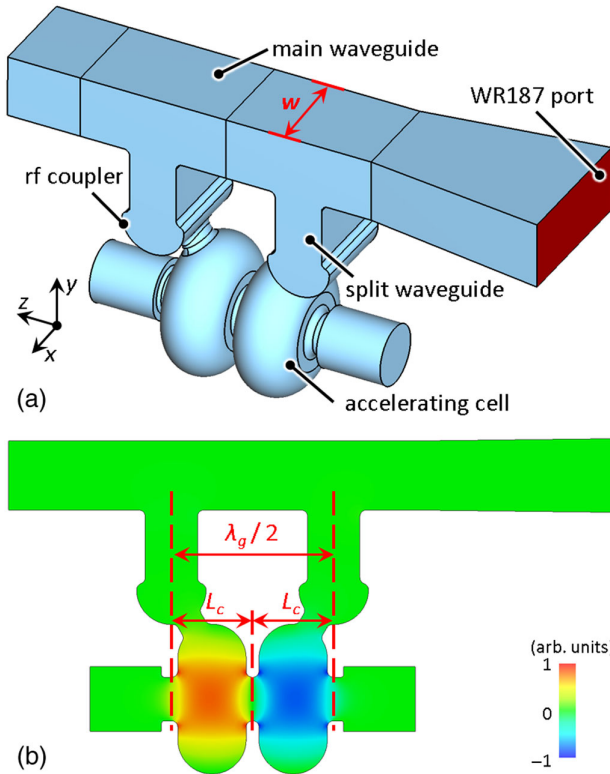


FIG. 1. (a) CST Microwave Studio model of the vacuum volume of the two-cell C-band rf cavity for the high-gradient testing; (b) distribution of the magnitude of E_z field in the cavity.

with the proton beam traveling with the speed of βc , where c is the speed of light in vacuum:

$$L_c = \frac{\beta\lambda}{2}, \quad (2)$$

with

$$\lambda = \frac{c}{f} \quad (3)$$

being the free-space wavelength.

The distance between the two distributed coupling split waveguides is determined by the periodicity of the multicell two-manifold distributed coupling accelerating structure with one distributed coupling waveguide feeding each accelerating cell [24]. To achieve the correct phase relationship between the two cells, this distance must be equal to the half of the wavelength of rf power in the main waveguide, λ_g :

$$\frac{\lambda_g}{2} = 2L_c, \quad (4)$$

$$\lambda_g = \frac{\lambda}{\sqrt{1 - (\frac{\lambda}{4w})^2}}. \quad (5)$$

Combining Eqs. (2), (4), and (5), we obtain the width of the main waveguide required to achieve properly phased distributed coupling:

$$w = \frac{\lambda}{\sqrt{4 - \frac{1}{\beta^2}}} > 0. \quad (6)$$

One important observation from Eq. (6) is that accelerator cavities with distributed coupling, which contain tens of cells, will have different widths w of the feeding waveguide for different proton beam energies (and values of β) along the booster linac. This is different from cavities with distributed rf coupling for electron linacs [24]. It is also worth noting that from Eq. (6) follows that a π mode, two-manifold distributed coupling linac can be designed only for $\beta > 0.5$, meaning that the proton beam propagates with a speed greater than half the speed of light (energy larger than 145 MeV).

The key parameters of the two-cell, π -mode, 5.712 GHz, standing wave test cavity for the pRad booster linac study are summarized in Table I. A few important features of this structure worth being highlighted are the relatively high-shunt impedance, especially compared to the TW $2\pi/3$, $\beta = 0.93$ structure with a similar aperture [25], low peak surface electric fields achieved by geometry optimization, and a relatively short filling time due to distributed coupling into the π mode.

Figure 2 shows the results of CST Microwave Studio computations for distributions of the electric and magnetic field magnitudes plotted on the surface of one of the two

TABLE I. Design parameters of the two-cell C-band test cavity.

Frequency, f	5712 MHz
Cell length, L_c ($\beta = 0.93$)	24.4 mm
Cell radius	21.9 mm
Beam aperture radius, a	6.5 mm
Ohmic Q factor, Q_0	13 150
Coupling Q factor, Q_{ext}	11 000
Shunt impedance (two cells), R_s	3.48 M Ω
Shunt impedance per unit length, r_s	71.4 M Ω /m
Accelerating field, E_0T	$38.25 \sqrt{P_{\text{peak}}(\text{MW})}$ MV/m
Peak surface electric field, E_p/E_0T	2.32
Peak surface magnetic field, $H_p \times Z_0/E_0T$	2.32
Filling time, 2τ	333 ns

cells. The maximum electric field (E_p) is located on the iris between the two cells and is 2.32 times the accelerating gradient. The maximum magnetic field (H_p) is located on the upper wall of the accelerating structure near the rf coupler, away from the beam iris, and the maximum magnitude of the magnetic field strength is equal to 2.32 times the accelerating gradient divided by the impedance of free space $Z_0 = 377 \Omega$. Both field distributions in Fig. 2 are plotted for accelerating field $E_0T = 80$ MV/m. The maximum peak electric field on the surface of the cavity and the maximum peak magnetic field are both the likely locations for the breakdowns, to be observed in the high-gradient testing [28]. The location of the maximum peak surface magnetic field is also where the maximum peak pulse surface heating will occur.

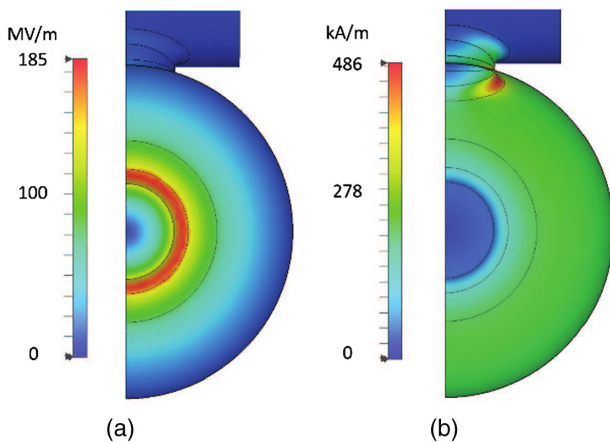


FIG. 2. (a) Magnitude of the electric field plotted on the surface of one cell of the two-cell cavity; (b) magnitude of the magnetic field plotted on the surface of one cell of the two-cell cavity. Both plots were computed with CST Microwave Studio for the accelerating field $E_0T = 80$ MV/m.

III. FABRICATION, COLD TEST, AND TUNING FOR THE TWO-CELL C-BAND TEST CAVITY

The test cavity was fabricated by Dymenso LLC [29] using precision machining. The CAD model for the cavity is shown in Fig. 3(a). The cavity was fabricated in two symmetrical halves that were brazed together with added stainless steel waveguide and vacuum flanges and water connectors. Water-cooling channels were made in the thick copper walls to allow for the operation at a high gradient with a repetition rate of 100 Hz used for breakdown studies at CERF-NM. Tuning fixtures with stainless steel tuning screws were added on the outer walls of the cells—two for each cell—to make small wall deformations for precise frequency tuning of the cavity. The photograph of the cavity after installation at CERF-NM is shown in Fig. 3(b).

The cavity was cold tested in a clean-room environment to minimize surface contamination. The initial frequency of the cavity before tuning was measured to be 5703.4 MHz in air, in good agreement with MWS simulated frequency of 5702.7 MHz, and about 7 MHz away from the target resonant frequency in air of 5710.3 MHz. The distribution

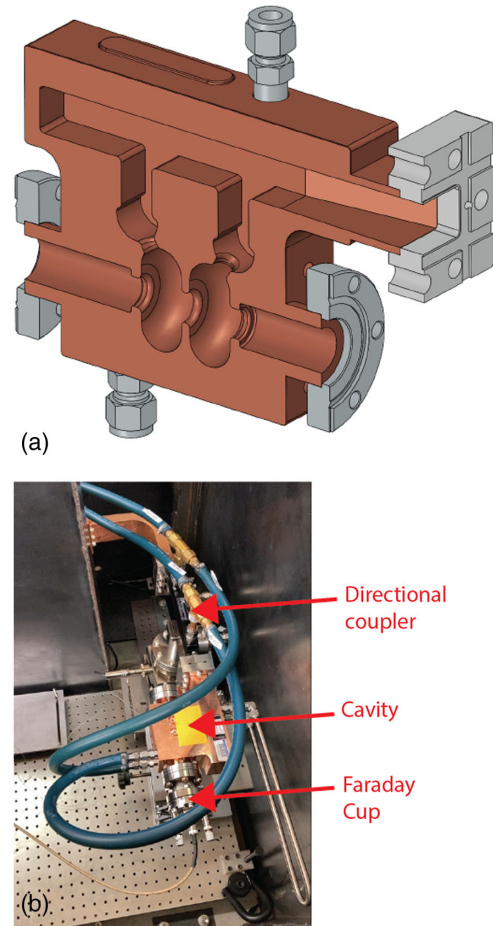


FIG. 3. (a) CAD model of the two-cell C-band rf cavity (longitudinal cross section); (b) photograph of the two-cell C-band rf cavity installed at the high-gradient test stand.

of the electric field on axis of the cavity was measured with a bead pull setup. The bead pull setup used the Ashaway USP 8/0 Monofilament Nylon thread, and the perturbation was provided by a 1-mm diameter desiccated super glue sphere, attached to the thread. The peak on-axis fields in the two cells were found to be of approximately equal magnitudes which indicates the high-precision quality of machining. The ohmic quality factor before tuning was found to be $Q_0 = 12\,820$, and the external quality factor measured before tuning was $Q_e = 10\,815$.

The cavity underwent several rounds of tuning that involved hitting and pulling the tuning screws with the sliding hammer. The goal of tuning was to raise the resonant frequency of the cavity to be closer to 5712 MHz in vacuum and again to equalize amplitudes of the electric field in two cavities. In the end, the cavity was tuned to the frequency of 5710.9 MHz in air, which corresponded to 5712.6 MHz in vacuum, well within the bandwidth of CERF-NM. The final measured quality factor of $Q_0 = 13\,238$ was slightly higher than the calculated value $Q_0 = 13\,150$ for copper walls with wall conductivity of $\sigma = 5.8 \times 10^7$ Sm/m, which was likely due to a small measurement error and also indicates very good surface and material quality of copper. The measured external quality factor $Q_e = 10\,137$ was slightly below the

TABLE II. Coupling parameters of the two-cell C-band test cavity.

Parameter	Simulated	Measured in cold-test
Frequency, f	5712.0 MHz	5710.9 MHz
Ohmic Q factor, Q_0	13 150	13 238
Coupling Q factor, Q_{ext}	11 000	10 137
Filling time, 2τ	333 ns	320 ns
Coupling β	1.195	1.306

calculated value of 11 000, so the final tuned cavity was overcoupled. The coupling curves and on-axis distribution of the electric field for the two-cell cavity as computed with CST Microwave Studio and as measured after the final tuning are plotted in Fig. 4. The coupling parameters for the cavity are summarized in Table II.

IV. HIGH-GRADIENT CONDITIONING OF THE TWO-CELL C-BAND TEST CAVITY

The high-gradient testing of the C-band two-cell proton booster test cavity was performed at the C-band Engineering Research Facility in New Mexico at LANL [27]. The CERF-NM is powered by a 50 MW, 5.712 GHz Canon klystron that produces 50 MW pulses with the pulse length between 300 ns and 1 μ s, repetition rate up to 200 Hz, and it is tunable within the operating bandwidth from 5.707 GHz to 5.717 GHz. The details of the test stand, its capabilities, and the results of some prior tests are reported in [30]. The cavity was installed at the end of the WR187 waveguide line inside of a lead box that provided radiation protection. The photograph of the experimental setup inside of the lead box is shown in Fig. 3(b). The directional coupler installed right before the cavity was used to record shapes of the forward and reflected rf power pulses. The dark current generated inside of the cavity under high-power conditioning was monitored using a Kimball Physics FC73a Faraday cup installed at one of the two beam pipe flanges of the cavity. The other beam pipe flange was blinded with a stainless-steel flange. Vacuum in the cavity was monitored with a vacuum gauge installed on the pumping port on the bottom of the directional coupler. A thermocouple was used to monitor the average temperature of the cavity during the high-gradient operation. The average temperature of the cavity increased slightly with higher rf power coupled into the structure but never exceeded 38°C.

The detailed procedure for the high-gradient cavity conditioning and breakdown rates mapping at CERF-NM is outlined in [26]. During the conditioning process, the forward and reflected pulse shapes were recorded continuously with a high-speed (2 GHz) oscilloscope. Typical forward and reflected power traces for the test are shown in Fig. 5. To compute the gradient and peak surface fields in the cavity for the given coupled power, we

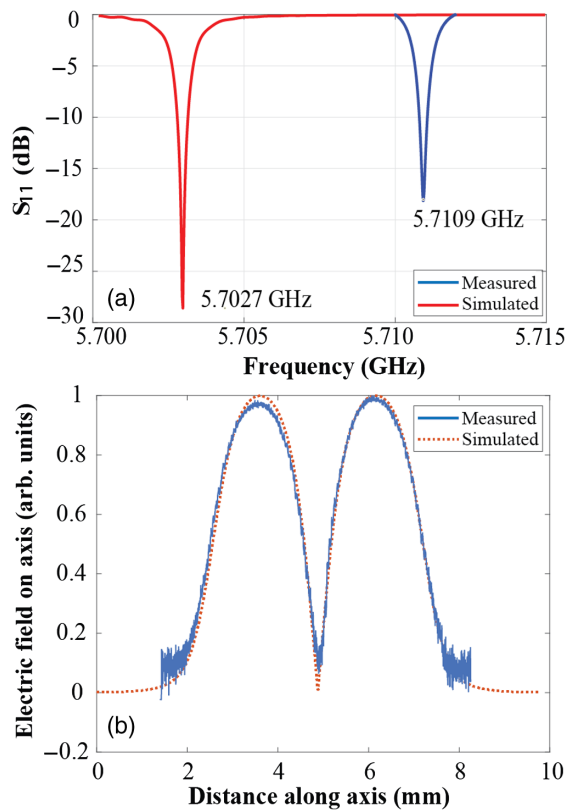


FIG. 4. (a) Reflection coupling curves for the two-cell C-band rf cavity in air as computed and measured after tuning; (b) electric field magnitude distribution on axis of the two-cell C-band rf cavity as computed and measured after tuning.

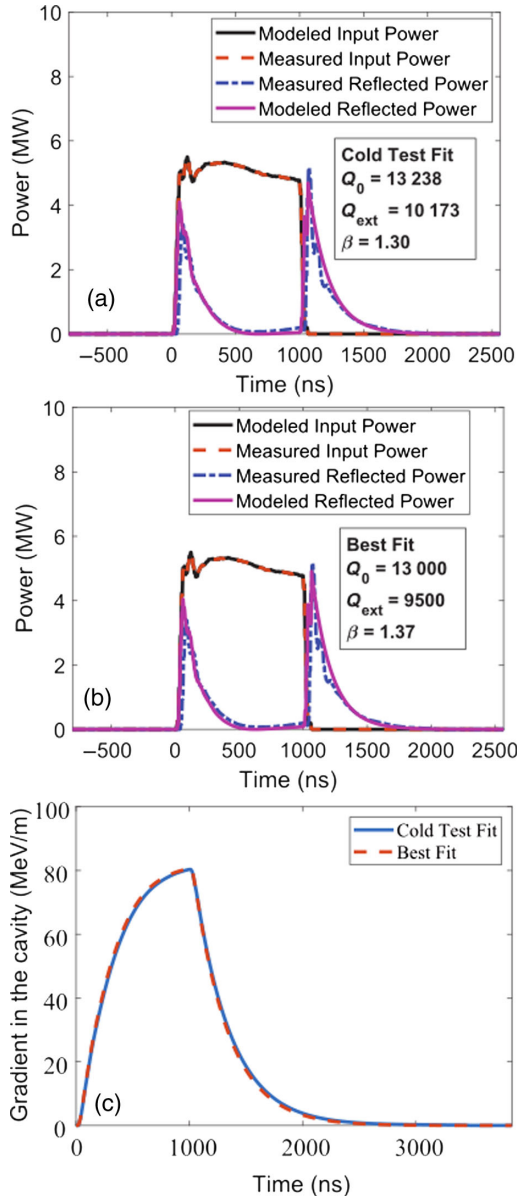


FIG. 5. Pulse shapes for the forward and reflected power at the cavity entrance measured in the experiment and calculated for the cavity with (a) Q factors measured in cold test and (b) the “best fit” Q factors. (c) The corresponding peak on-axis gradient as a function of time for both scenarios.

used the model that utilized constant Q factors and resonant frequencies to predict reflected pulse shapes and compute the fields based on the measured forward pulse shapes [31]. Figure 5(a) shows the comparison between the measured and modeled pulse shapes based on the Ohmic $Q_0 = 13\,150$ and external $Q_e = 10\,137$ measured in the cold test. Very good agreement between the modeled and computed pulse shapes is observed. We then made adjustments to the Q factors to find an even better fit between the measured and computed pulse shapes following the same procedure as described in [26]. The best fit was obtained for the values of the Ohmic $Q_0 = 13\,000$ and external $Q_e = 9\,500$, which

are also in good agreement with theoretical predictions, the curves for these Q factor values are plotted in Fig. 5(b). The coupling β computed from the pulse shapes is also in good agreement with the theory. The accelerating gradient in the cavity computed with the linear equivalent circuit model is plotted in Fig. 5(c) as a function of time. The maximum gradient in the cavity is achieved at the time corresponding to the end of the forward power pulse.

The cavity was conditioned to the maximum gradient of 100 MV/m which corresponded to approximately 8.3 MW of peak forward power coupled into the cavity. The maximum power that we could couple into the cavity was limited by the klystron interlock that shut down the klystron when the power reflected back to the klystron in the event of rf breakdown exceeded 2 MW.

V. BREAKDOWN MEASUREMENTS IN THE C-BAND TEST CAVITY

Finally, we collected the rf breakdown statistics for the two-cell test cavity following the procedure described in Ref. [26]. The probabilities of the rf breakdown were measured for several different accelerating gradients between 75 and 100 MV/m. The results of breakdown testing are summarized in Fig. 6. Figure 6(a) shows probabilities of breakdown plotted versus the magnitude of the peak electric field (E_p) on the surface of the cavity. Figure 6(b) shows probabilities of breakdown plotted versus the magnitude of the peak magnetic field intensity (H_p) on the surface of the cavity. Figure 6(c) shows probabilities of breakdown plotted versus the average accelerating gradient on the axis of the cavity. We found that the structure achieved moderately high gradients (up to 100 MeV/m) with breakdown probabilities below 10^{-3} /pulse/m. For the 100 MeV/m accelerating gradient, the peak surface electric field in the cavity was close up to 230 MV/m, and the peak surface magnetic field intensity was slightly above 600 kA/m.

Compared to the results of high-gradient testing of other C-band accelerating cavities, for example, to those reported in [26], we see that cavities with different shapes achieve similar breakdown probabilities of 10^{-3} 1/pulse/m for notably higher peak surface electric fields (above 300 MV/m) and notably lower peak surface magnetic field intensities (450 kA/m). From this, we infer that in this two-cell C-band test cavity, the breakdown rate was mostly dominated by the high-surface magnetic fields and the pulse heating. This conclusion is also confirmed by the calculations of the peak surface temperature rises for various levels of the input power plotted in Fig. 7. Figure 7 displays the temperature rise on the surface of the cavity due to pulse heating during the high-gradient rf pulse. For the maximum measured accelerating field of 100 MV/m, the peak pulse heating exceeds 80 K, which is considered higher than the maximum allowable peak pulse heating for high-gradient operations and leads to increased probabilities of rf breakdown [28].

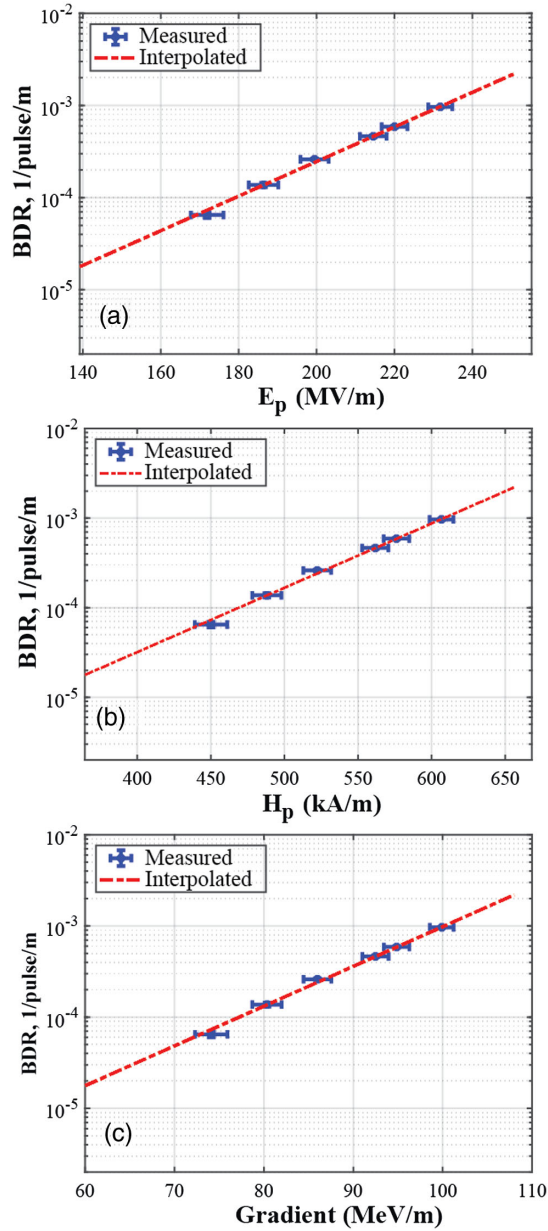


FIG. 6. Measured breakdown rates plotted (a) as a function of peak electric field (E_p) and (b) peak magnetic field (H_p) on the surface of the accelerator structure, and (c) accelerating gradient. The trend lines are the data fitted to an exponential fit. The breakdown data were collected for the rf pulse length of $1 \mu\text{s}$.

The target accelerating gradient in the C-band section of the booster linac for pRad upgrade is 40 MeV/m [14]. By extrapolating data in Fig. 6, we estimate that at this gradient, the expected breakdown rate is about 2×10^{-6} 1/pulse/m. This means that the whole 50-m-long C-band section of the booster linac would have the breakdown probability of 10^{-4} 1/pulse with this cavity design, which is very good considering that pRad operates at a very low duty factor. However, one should note that in the two-cell test cavity, each coupler diverts to its cell one-half of the total rf

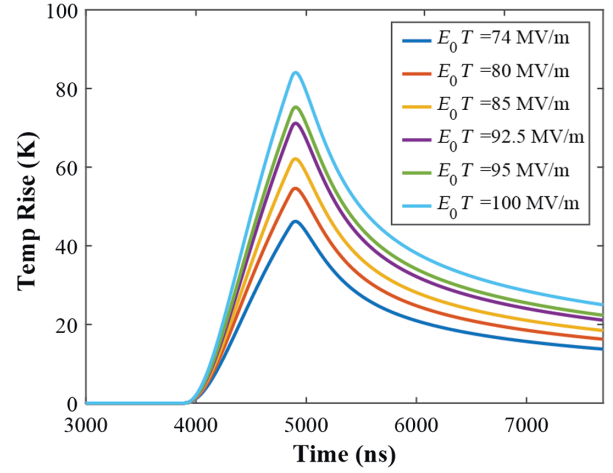


FIG. 7. Peak surface temperature rise as a function of time for rf pulse length of $1 \mu\text{s}$ and different accelerating fields in the cavity. Note that the peak temperature rise increases linearly with accelerating fields for a given pulse length.

power from the waveguide: this is why these couplers are so large compared to the cell sizes (see Fig. 1). In a multicell accelerating structure with distributed rf coupling, the couplers will be much smaller, which will likely further reduce peak surface magnetic fields and the breakdown rates.

VI. CONCLUSION

In summary, this paper reported the results of design, construction, and testing of a C-band two-cell accelerating cavity with distributed rf coupling that serves as a prototype for an accelerating cavity for the high-gradient booster linac for the 3 GeV proton radiography upgrade at Los Alamos Neutron Science Center. The measurements of the fabricated cavity were in good agreement with simulations, which validated the design. The cavity is capable of operating at the desired gradient of 40 MeV/m with a rather low probability of breakdown. It was concluded that multicell accelerating structures with distributed rf coupling for pRad booster linac are feasible. The final design of the multicell distributed coupling accelerating structure must focus on the optimization of the cavity shape, and in particular, the rf coupler region to reduce the peak surface magnetic fields in the cavity and further reduce breakdown probabilities.

It is worth noting that the proposed pRad booster linac will require significantly less rf power and operate with a smaller breakdown probability at the gradient of 40 MeV/m if the structures are cooled to very low temperatures with liquid nitrogen [32,33]. With the very low duty factor required for pRad, liquid nitrogen will experience minimal heating due to Ohmic loss and cryotemperatures can be maintained with simple daily liquid nitrogen refills. Thus, one of our future research priorities is to further investigate the

cryocooled NCRF solution for the pRad booster linac system development.

Finally, the C-band pRad booster linac test cavity research reported in this paper was conducted in synergy with ongoing, collaborative C-band accelerator research activities at LANL and elsewhere. While the C-band distributed coupling linac continues to be refined for the Cool Copper Collider (C³) initiative [34,35], the technologies developed in the C³ program have inspired other applications, for example, in radiation therapy devices [26,36,37].

ACKNOWLEDGMENTS

This work was supported by the U.S. Department of Energy, through the Laboratory Directed Research and Development (LDRD) Program at Los Alamos National Laboratory, under Project No. 20210048ER.

-
- [1] A. Saunders, Los Alamos National Laboratory, Los Alamos, NM, Technical Report No. LA-UR-17-21683, 2017, <https://doi.org/10.2172/1345179>.
- [2] K. E. Kippen, R. D. Fulton, E. Brown, W. T. Buttler, A. J. Clarke, K. K. Kwiatkowski, F. S. Mariam, F. e. Merrill, C. Morris, R. T. Olson, and M. Zellner, AOT & LANSCE focus: Proton radiography facility, Los Alamos National Laboratory, Los Alamos, NM, Technical Report No. LA-UR-13-24376, 2013.
- [3] R. W. Garnett, F. E. Merrill, J. F. O'Hara, D. E. Rees, L. G. Rybarcyk, T. Tajima, and P. L. Walstrom, in *Proceedings of the 3rd International Particle Accelerator Conference, New Orleans, LA, 2012* (IEEE, Piscataway, NJ, 2012).
- [4] F. E. Merrill, E. Campos, C. Espinoza, G. Hogan, B. Hollander, J. Lopez, F. G. Mariam, D. Morley, C. L. Morris, M. Murray, A. Saunders, C. Schwartz, and T. N. Thompson, *Rev. Sci. Instrum.* **82**, 103709 (2011).
- [5] C. L. Morris, E. Ables, K. R. Alrick, M. B. Aufderheide, P. D. Barnes Jr, K. L. Buescher, and D. J. Cagliostro, *J. Appl. Phys.* **109**, 104905 (2011).
- [6] B. Franzke, *Nucl. Instrum. Methods Phys. Res., Sect. B* **24–25**, 18 (1987).
- [7] K. Blasche, U. Blell, O. Boine-Frankenheim, P. Forck *et al.*, GSI Sci. Rep. 184 (2000), <https://repository.gsi.de/record/53531/files/GSI-Report-2001-1.pdf?version=1>.
- [8] P. Spiller, R. Balss, P. Bartolome, J. Blaurodck *et al.*, *J. Instrum.* **15**, T12013 (2020).
- [9] P. L. Walstrom and E. G. Cook, in *Proceedings of the 19th Particle Accelerator Conference, Chicago, IL, 2001* (IEEE, Piscataway, NJ, 2001).
- [10] Y. K. Batygin, D. V. Gorelov, S. S. Kurennoy, J. W. Lewellen, N. A. Moody, and L. J. Rybarcyk, in *Proceedings of the 12th International Particle Accelerator Conference, IPAC'21, Campinas, SP, Brazil* (JACoW, Geneva, Switzerland, 2021), p. 1894.
- [11] S. S. Kurennoy, A. J. Jason, F. L. Krawczyk, and J. Power, in *Proceedings of the Particle Accelerator Conference, Vancouver, BC, Canada, 1997* (IEEE, New York, 1997).
- [12] S. S. Kurennoy, L. J. Rybarcyk, and V. A. Dolgashev, in *Proceedings of the 28th Linear Accelerator Conference, East Lansing, MI* (JACoW, Geneva, Switzerland, 2016), p. 280.
- [13] S. S. Kurennoy and Y. K. Batygin, in *Proceedings of the 12th International Particle Accelerator Conference, IPAC'21, Campinas, SP, Brazil* (JACoW, Geneva, Switzerland, 2021), p. 693.
- [14] Y. K. Batygin and S. S. Kurennoy, in *Proceedings of the 4th North American Particle Accelerator Conference, Albuquerque, NM* (JACoW, Geneva, Switzerland, 2022), p. 891.
- [15] S. S. Kurennoy, Y. K. Batygin, and E. R. Olivas, in *Proceedings of the 20th Advanced Accelerator Concepts Workshop AAC2022, Hyatt Regency Long Island, Hauppauge, NY* (IEEE, New York, 2022).
- [16] D. Alesini *et al.*, *Nucl. Instrum. Methods Phys. Res., Sect. A* **837**, 161 (2016).
- [17] D. Alesini *et al.*, *Phys. Rev. Accel. Beams* **20**, 032004 (2017).
- [18] D. Alesini *et al.*, *Phys. Rev. Accel. Beams* **23**, 042001 (2020).
- [19] T. Sakurai, H. Ego, T. Inagaki, T. Asaka, D. Suzuki, S. Miura, and Y. Otake, *Phys. Rev. Accel. Beams* **20**, 042003 (2017).
- [20] W. Fang, Q. Gu, X. Sheng *et al.*, *Nucl. Instrum. Methods Phys. Res., Sect. A* **823**, 91 (2016).
- [21] A. Degiovanni, U. Amaldi, R. Bonomi, M. Garlasché, A. Garonna, S. Verdú-Andrés, and R. Wegner, *Nucl. Instrum. Methods Phys. Res., Sect. A* **657**, 55 (2011).
- [22] S. Verdú-Andrés, U. Amaldi, and Á. Faus-Golfe, *Journal of Radiation Research* **54**, i155 (2013).
- [23] A. Degiovanni, R. Bonomi, M. Garlasché, S. Verdú-Andrés, R. Wegner, and U. Amaldi, *Nucl. Instrum. Methods Phys. Res., Sect. A* **890**, 1 (2018).
- [24] S. G. Tantawi, Mamdouh Nasr, Zenghai Li, Cecile Limborg, and Philipp Borchard, *Phys. Rev. Accel. Beams* **23**, 092001 (2020).
- [25] S. S. Kurennoy, Y. K. Batygin, E. R. Olivas, E. I. Simakov, H. Xu, and M. Zuboraj, in *Proceedings of the 14th International Particle Accelerator Conference, IPAC-2023, Venice, Italy* (JACoW, Geneva, Switzerland, 2023), p. 2205.
- [26] M. Schneider, V. Dolgashev, J. W. Lewellen, S. G. Tantawi, E. A. Nanni, M. Zuboraj, R. Fleming, D. Gorelov, M. Middendorf, and E. I. Simakov, *Appl. Phys. Lett.* **121**, 254101 (2022).
- [27] D. Gorelov, R. L. Fleming, J. W. Lewellen, M. E. Middendorf, D. Perez, M. E. Schneider, E. I. Simakov, and T. Tajima, in *Proceedings of the 2021 Particle Accelerator Conference (IPAC'21), Campinas, Brazil* (2021).
- [28] E. I. Simakov, V. A. Dolgashev, and S. G. Tantawi, *Nucl. Instrum. Methods Phys. Res., Sect. A* **907**, 221 (2018).
- [29] Dymenso LLC (2022), <https://www.dymenso.com/>.
- [30] E. I. Simakov, A. M. Alexander, D. V. Gorelov, T. W. Hall, M. E. Middendorf, D. Rai, T. Tajima, and M. R. A. Zuboraj, in *Proceedings of the 4th North American*

- Particle Accelerator Conference, Albuquerque, NM* (JACoW, Geneva, Switzerland, 2022).
- [31] T.P. Wangler, *RF Linear Accelerators* (John Wiley and Sons, New York, 1998).
- [32] A.D. Cahill, J.B. Rosenqweig, V.A. Dolgashev, S.G. Tantawi, and S. Weathersby, *Phys. Rev. Accel. Beams* **21**, 102002 (2018).
- [33] M. Nasr, E. Nanni, M. Breidenback, S. Weathersby, M. Oriunno, and S. Tantawi, *Phys. Rev. Accel. Beams* **24**, 093201 (2021).
- [34] E. A. Nanni, M. Breidenback, Z. Li, C. Vernieri *et al.*, *J. Instrum.* **18**, P09040 (2023).
- [35] C. Vernieri, C. Nanni, S. Dasu, M.E. Peslin *et al.*, *J. Instrum.* **18**, P07053 (2023).
- [36] P.G. Maxim, S.G. Tantawi, and B.W. Loo, Jr., *Radiot. Oncol.* **139**, 28 (2019).
- [37] X. Lu, Z. Li, V. Dolgashev, G. Bowden, A. Sy, S. Tantawi, and E. A. Nanni, *Rev. Sci. Instrum.* **92**, 024705 (2021).